Facile coating of Co3O4 on open-cell metallic foam for N2O catalytic decomposition

Phuoc Hoang Ho, Katarzyna Świrk, Giancosimo Sanghez de Luna, Magdalena Jabłońska, Francesca Ospitali, Francesco Di Renzo, Gérard Delahay, Giuseppe Fornasari, Angelo Vaccari, Regina Palkovits, et al.

Facile coating of Co_3O_4 on open-cell metallic foam for N_2O catalytic decomposition Phuoc Hoang Ho[a,b,§,†,*], Katarzyna Świrk[c,§], Giancosimo Sanghez de Luna[a,§], Magdalena Jabłońska[b,d,e], Francesca Ospitali[a], Francesco Di Renzo[c], Gérard Delahay[c,***], Giuseppe Fornasari[a], Angelo Vaccari[a], Regina Palkovits[b,d], Patricia Benito[a]** [a] Dipartimento di Chimica Industriale "Toso Montanari", Università di Bologna, Viale Risorgimento 4, 40136, Bologna, Italy [b] Institut für Technische und Makromolekulare Chemie, RWTH Aachen University, Worringerweg 2, 52074 Aachen, Germany [c] ICGM, Université de Montpellier, CNRS, ENSCM, Pôle Recherche Balard, 1919 Route de Mende, 34090 Montpellier, France [d] Center for Automotive Catalytic Systems Aachen, RWTH Aachen University, Schinkelstr. 8, 52062 Aachen, Germany [e] Institute of Chemical Technology, Universität Leipzig, Linnéstr. 3, 04103 Leipzig, Germany [§] Equal contribution

† Present address: Chemical Engineering, Competence Centre for Catalysis, Chalmers University of Technology, SE-412 96, Gothenburg, Sweden

• phuoc@chalmers.se

Chemical Engineering, Competence Centre for Catalysis, Chalmers University of Technology, SE-412 96, Gothenburg, Sweden

** patricia.benito3@unibo.it

Dipartimento di Chimica Industriale "Toso Montanari" Università di Bologna

Viale Risorgimento 4,

40136, Bologna, Italy

*** gerard.delahay@enscm.fr

ICGM, Université de Montpellier, CNRS, ENSCM, Pôle Recherche Balard, 1919 Route de Mende, 34090 Montpellier, France

Abstract

Co_3O_4 coated on open-cell metallic foams (, merging catalytic activity of Co_3O_4 and advantages derived from the geometry of the support), are promising for environmental applications such as the decomposition of N_2O (deN_2O). This study demonstrates how ~~it is possible to~~ easily and reproducibly prepare a well-adhered layer of Co_3O_4 by the electrosynthesis of $Co(OH)_2$ followed by thermal treatment (600 °C). with Aa similar specific surface area as the materials prepared with the precipitation method (~ 22 m^2 g^{-1} $_{coating}$), and controlled thickness on FeCrAlloy open-cell foams of different porosity and dimension are achieved. by the electrosynthesis of $Co(OH)_2$ followed by thermal treatment (600 °C). The obtained structured catalysts show stable performance activity after three cycles of catalytic decomposition of N_2O between 250 and 550 °C. , with a The materials reached similar T_{50} of approximately 460 °C, which is comparable to the combustion or precipitated catalysts but provides a lower pressure drop. Under the operating conditions with a sequential test, the presence of NO and/or O_2 inhibits partially the catalytic performance activity of the structured catalysts while the presence of H_2O showed a slight enhancement in the N_2O conversion at a temperature above 450 ºC.

Graphical abstract

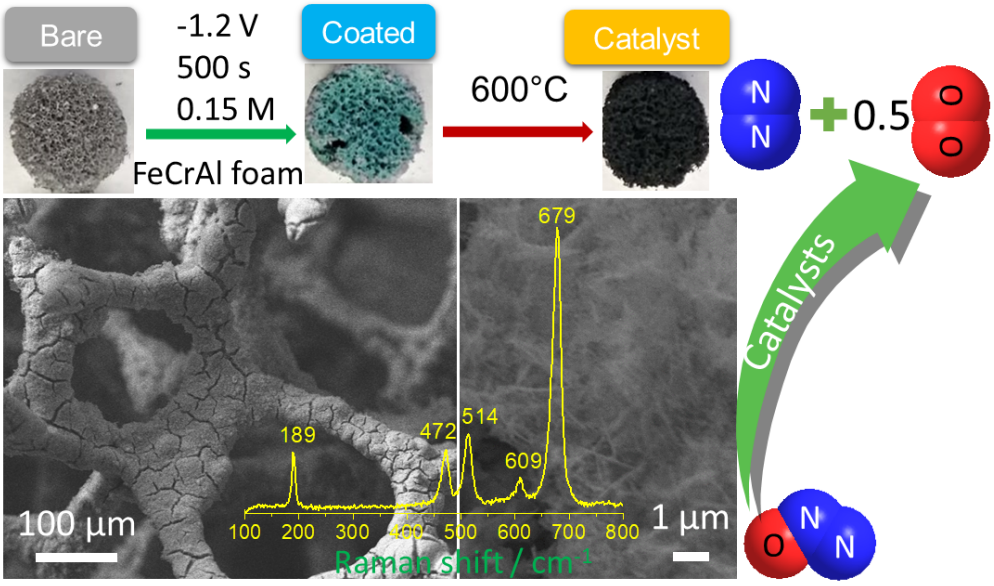

Highlights

- $Co(OH)_2$ layer is easily coated on FeCrAlloy open-cell foam by electrodeposition.
- Calcination at 600 °C results in a stable coating of Co_3O_4 with a high specific surface area.
- Catalyst loading can be tailored by synthesis time and electrolytic concentration.
- T_{50} for deN_2O is in a range of 477 – 543 °C with in the presence of O_2, NO, and H_2O.
- Promising use in other energy and environmental applications.

Keywords: Electrodeposition, $Co(OH)_2$, Co_3O_4, open-cell metallic foam, N_2O decomposition.

1. Introduction

Open-cell foams are a special member of the 3D structured support family with high porosity (void fraction 90-95%) and geometrical surface area (e.g., 7800 m^2 m^{-3} for 450 μm cell-size with 85% porosity); hence the structured catalysts based on open-cell foams offer many advantages in terms of mass and heat transfer together with a low-pressure drop [1]. Such advantages are promising for environmental applications in which the processes operate at high GHSV and are exothermic. Open-cell foams are now commercialized with various compositions, from ceramic- to metallic- or alloy-based materials. Metallic or alloy foams with high thermal or electrical conductivity offer additional advantages in mechanical strength and heat transfer for heterogeneous catalysis [2, 3]. A key point for those applications is the development of a technique to coat the structured supports with a stable layer of catalytic materials. Conventional wash coating or dip coatings are challenging because of significant differences in properties between the metallic foam and ceramic-coating layer as well as the pore blockage. The latter is important for foams with small pores, although spin coating has been reported to solve this issue [4]. Spin coating follows almost the same procedure as wash-coating/dip-coating for the preparation of the catalyst slurry, except the last step uses spinning to provide better distribution and to remove excess coating slurry [4]. Although this technique has been found to significantly improve the properties and hence the catalytic activity of the structured catalysts, it may still face the problem of modification of catalytic materials during the slurry preparation [5-7].

Besides spin coating, electrodeposition has been proposed by some of us to coat hydrotalcite- or ceria-derived materials for syngas production and environmental applications [8, 9]. Herein we extend the method to coat a cobalt-based material on small pore FeCrAlloy foams for the preparation of open-cell foam structured catalysts carrying a Co_3O_4 material. Structured supports carrying on cobalt-based materials have found application in both electrocatalysis [10-13] and heterogeneous catalysis [14-17]. A few studies have reported the preparation of Co_3O_4 or $Co(OH)_2$ on Ni foams but only as a rather thin film for water oxidation or supercapacitors [10, 13]. Such thin coating, few microns, lacks the mass loading required for heterogeneous catalysis purposes. In addition, Co_3O_4-coated ceramic honeycomb monoliths and foams have been used for N_2O abatement [14, 17-19], partial oxidation of ethanol [15], combustion of volatile organic compounds [16], methane oxidation [20], and Fischer–Tropsch synthesis [21-24]. Our previous study reported that structured catalysts containing an Rh-based coating were promising for the catalytic decomposition of N_2O [25]. However, moving from noble metals toward transition metals, the development of catalysts has gained more interest due to the higher cost of the former than the latter. To the best of our knowledge, the use of Co_3O_4 coated on open-cell metallic foams is rare, especially for the important process of N_2O decomposition. Nitrous oxide is a strong greenhouse gas, from plants producing nitric acid or adipic acid, the emissions of which must be reduced to meet the 2 °C limit of global temperature increase [26].

This study introduces the electrodeposition of a relatively thick layer of $Co(OH)_2$ up to 15-18 μm on FeCrAlloy open-cell foam of high pore density (80 PPI), which is then transformed into Co_3O_4 by calcination at 600 °C. The coating layer and the final structured catalysts are characterized to study morphology, specific surface area, and redox properties in comparison

with precipitated Co_3O_4. A selected application of the structured catalyst for N_2O decomposition has been tested.

2. Experimental

2.1 Catalyst preparation

Cylindrical pieces of FeCrAlloy open-cell foam (diameter 8 mm x height 7 mm, supplied by Poivair, denoted as foam type I) were cut from a commercial panel (nominal 80 pores per inch (PPI), panel thickness 7 mm). Cobalt hydroxides were in situ coated on the foam in short times by one-step electrodeposition using a double compartment electrochemical cell, flushing the electrolyte with a flow rate of 2 mL min^{-1}. Detailed information on the instrument can be found elsewhere [27]. The samples were prepared at a cathodic potential of -1.2 V vs SCE using different concentrations of $Co(NO_3)_2$ aqueous solutions (0.06 – 0.15 M) and synthesis times (500 – 1500 s). As a general trend in electrosynthesis, either synthesis time or electrolytic concentration can influence the loading and crystallinity of the coated materials [28]. Herein, to demonstrate how the coating loading can be controlled by the electrosynthesis, three selected samples prepared at 0.06 M – 1500 s, 0.10 M – 1000 s, and 0.15 M – 500 s were shown. The electrodeposited samples were washed thoroughly with distilled water before drying at 40 °C for 24 h. The samples were eventually calcined at 600 °C for 6 h in static air with a ramp rate of 10 °C min^{-1} and denoted as Co-0.15, Co-0.10, and Co-0.06, wherein the number referred to the concentration of the electrolytes. To check if the method can work on different types of metallic foams, some samples were also synthesized using another FeCrAlloy support (1.6 mm thickness x 9 mm diameter, nominal cell size 450 μm (approximately 120 PPI), supplied by Alantum, denoted as foam type II) at -1.2 V, 0.15 M, and 250 s.

For comparison purposes, the Co_3O_4 powder catalyst was also prepared by precipitation. A 1.0 M nitrate solution of $Co(NO_3)_2$ was dropwise introduced into a beaker containing 100 mL of 1.0 M Na_2CO_3 solution. The pH was adjusted at 10 ± 0.1 by 1.0 M NaOH solution. The resulting slurry was aged for 0.5 h at 60 °C, filtered, and washed thoroughly with warm distilled water (60 °C). The final products were dried at room temperature for 24 h and subsequently calcined at 600 °C for 6 h. The powder catalyst was then pelletized and sieved to collect a fraction of particle size from 0.25 to 0.50 mm for the catalytic test.

2.2 Characterization techniques

X-ray diffraction (XRD) measurement was performed using a PANalytical X'Pert diffractometer equipped with a copper anode (λ =1.5418 Å) and a fast X'Celerator detector. The pattern was recorded from 10 to 80° of 2θ with a step size of 0.067° and a counting time of 60 s.

Scanning electron microscopy (SEM) coupled to energy dispersive spectrometry (EDS) was performed by using an EP EVO 50 Series Instrument (EVO ZEISS) equipped with an INCA X-act Penta FET® Precision EDS microanalysis and INCA Microanalysis Suite Software (Oxford

Instruments Analytical) to provide images of the spatial variation of elements in a sample. The accelerating voltage was 20 kV and the spectra were collected for 60 s.

The specific surface area of the catalysts was determined by N_2 adsorption/desorption at -196 °C. The measurements were carried out using a Micromeritics ASAP 2020 instrument. Two coated foams containing approximately 30 mg of the coating were used for each measurement. Samples were degassed under vacuum < 30 μm Hg, heated up to 150 °C, and maintained for 30 min before performing the measurement. The specific surface area (S_{BET}) was calculated using the Brunauer-Emmett-Teller (BET) multiple-point method in the relative pressure range p/p^0 from 0.05 to 0.3.

Micro-Raman measurements were performed in a Renishaw Raman Invia configured with a Leica DMLM microscope. The available sources are an Ar^+ laser (514.5 nm, P_{max} = 30 mW) and a diode-laser (780.0 nm, P_{max} = 300 mW). The system was equipped with edge filters to cut Rayleigh scattering, monochromators (1800 lines/mm for Ar^+ laser, and 1200 lines/mm for diode laser) and a Charge-Coupled Device (CCD) thermoelectrically cooled (203 K) detector. Measurements were performed with the Ar^+ Laser (514.5 nm) at power level P_{out}= 3 mW (10% power). Each spectrum was recorded by four accumulations (30 s for each).

Hydrogen temperature-programmed reduction (H_2-TPR) was performed in an AutoChem II (Chemisorption analyzer, Micromeritics). The catalyst (two coated foams) was firstly outgassed at 150 °C under 30 mL min^{-1} of He for 30 min. After cooling to 30 °C under He gas, the carrier gas was switched to 5% H_2/Ar (v/v) at 30 mL min^{-1}. When the baseline was stable, the temperature was increased to 900 °C with a ramp of 10 °C min^{-1}. The amount of H_2 consumed was measured using a thermal conductivity detector (TCD). Water vapor was removed from effluent gas by the means of a cold trap placed in an ice-water bath.

2.3 Catalytic test

The catalytic tests for the decomposition of N_2O (deN_2O) were performed in a quartz reactor (ID 8 mm) containing two foams of catalyst (diameter 8 mm and height 7 mm). Prior to each experiment, the structured catalysts were outgassed at 500 °C for 0.5 h under 80 mL min^{-1} of N_2 and then cooled down to 50 °C. After that, 80 mL min^{-1} of a gas mixture containing 1000 ppm N_2O in N_2 as balance was switched on to pass through the catalyst bed with GHSV = 6800 h^{-1} (or WHSV = 160,000 L kg^{-1} h^{-1} calculated based on 30 mg coating materials). The reaction was carried out at atmospheric pressure and in a range of temperatures from 50 °C to 500 °C (in absence of inhibitor) or 600 °C (in presence of inhibitors) with an interval of 50 °C. At each temperature, the reaction was stabilized for 0.5 h before being sent for quantification of N_2O concentration. The gas composition in the outlet stream was analyzed by infrared spectroscopy using an Agilent Cary 660 equipped with a Pike 2 m heated gas cell.

For type II foam activity testing, five foam discs containing a total of about 24 mg of the coating were loaded into a quartz reactor (inner diameter 9 mm). The catalyst was pretreated at 550 °C for 1 h under a flow of He (30 mL min^{-1}) and then cooled to 250 °C. Different gas compositions

(balance with He) were used for the tests including: I) [N_2O] = 2500 ppm, ii) [N_2O] = 2500 ppm + [O_2] = 2%; iii) [N_2O] = 2500 ppm + [NO] = 500 ppm; iv) [N_2O] = 2500 ppm + [NO] = 500 ppm + [O_2] = 2%, and v) [N_2O] = 2500 ppm + [H_2O] = 3.6% + [O_2] = 2%. Water was added before being mixed with the N_2O/He gas flow. The by passing the O_2/He gas flow passed through a temperature-controlled saturator, containing water liquid, before being mixed with the N_2O/He gas flow. A series of tests were performed in sequential order as shown in Figure S1. The gas compositions were analyzed by a quadruple mass spectrometer (Pfeiffer Omnistar) equipped with Channeltron and Faraday detectors (0–200 amu).

The conversion of N_2O ($X(N_2O)$) was determined according to $X(N_2O) = ([c(N_2O)_{in} - c(N_2O)_{out}]/c(N_2O)_{in})x100\%$, where: $c(N_2O)_{in}$ and $c(N_2O)_{out}$ – concentration of N_2O in the inlet gas, and concentration of N_2O in the outlet gas.

The reaction rate (in term of a number of N_2O molecules converted on a defined surface area (1 m2) of the catalyst during a given time (1 s)) was calculated by the following equation: $r\ (mol.\cdot m^{-2}\cdot.s^{-1}) = n.\cdot(X/100)/(m.\cdot S_{BET})$, where n – molar flow rate of N_2O [$mol.s^{-1}$], m – catalyst weight [g], S_{BET} – specific surface area [$m^2.\cdot g^{-1}$] and X – N_2O conversion [%] [29].

The apparent activation energy was calculated from the slope of linear regression derived from the Arrhenius equation $k = A \cdot e^{-(Ea/RT)}$, where k was calculated from the kinetic model for the flow reactor with an assumption of the first-order reaction $k\tau = X_{N_2O}/(100\text{-}X_{N_2O})$ [30]. In which k (s^{-1}) is the kinetic rate constant, A is the pre-exponential factor and it has the unit of s^{-1} for the first-order reaction, E_a (J mol^{-1}) is the apparent activation energy, R (J $\cdot mol^{-1}\ K^{-1}$) is the ideal gas law constant, T (K) is temperature, τ (s) is space-time (approximate 0.38 s) which is determined from the ratio between the volume of the catalytic bed (about 0.5 cm^3) and total flow of 1.33 $cm^3\ s^{-1}$.

3. Results and Discussion

3.1 Catalyst physico-chemical characterizations

The electrodeposition of hydroxides on the surface of a metallic foam is based on the generation of OH^-, mainly from the reduction of nitrate and/or water at the interface of cathode-electrolyte, by applying a cathodic potential and then consumption of those OH^- by chemical precipitation with available cations at the cathode vicinity [31]. Such reduction processes consume electrons and the consumption rate is represented by the current transient curves as shown in Figure 1.

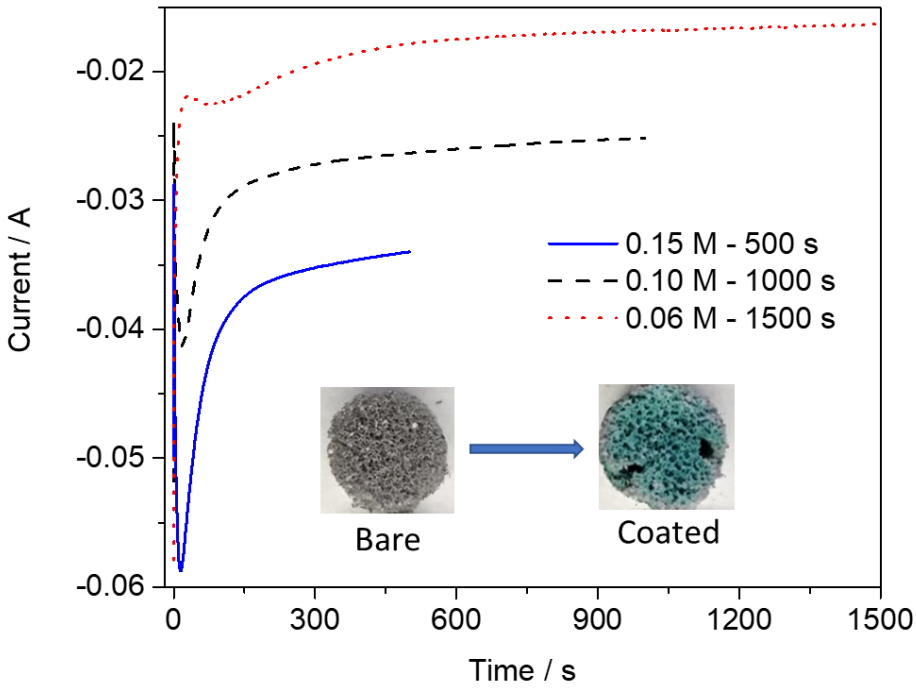

Figure 1. Transient current curves recorded during the electrodeposition of $Co(OH)_2$ on foam type I at -1.2 V vs SCE. The insets show optical images of bare foam and the coated foam prepared in 0.15 M $Co(NO_3)_2$ electrolytes for 500 s.

Increasing the concentration of electrolyte from 0.06 to 0.15 M led to higher nitrate reduction and hence resulted in an increase of current from 18 to 34 mA (Figure 1). This trend is in agreement with our previous work on the electrodeposition of Mg-Al hydrotalcite compounds [28]. An important question is whether such nitrate (and also water) reduction currents generate a pH high enough for the precipitation of $Co(OH)_2$. This pH value is around 7.3 – 7.5 for concentrations 0.15 – 0.06 M of $Co(NO_3)_2$, respectively (calculated from equilibrium solubility constant $K_s = 6.93 \cdot *10^{-15}$ [32]). , aAlthough the electrosynthesis on the foam could favor heterogeneous precipitation instead of homogeneous one inducing the deposition of uniform and small particles due to the fast and uniform increase of pH near the foam surface [33]. It should be noted that pH measured near the cathode is a balance of generation and consumption of OH^- . and, aAfter an initial pH increase from the acidic value of the electrolyte, it stabilizes to equilibrium values for precipitation of the hydroxides. For instance, pH values around 8.5 – 9.0 were measured during the electrodeposition of Mg/Al hydrotalcite-like compounds at -1.2 V vs SCE in the bath containing electrolytes with a concentration of 0.03 – 0.1 M. Thus, it is expected that the synthesis conditions in this work (-1.2 V vs SCE, electrolytic concentration 0.06 – 0.15 M) generated a pH high enough for precipitation of $Co(OH)_2$. Indeed a blue coating, a typical color for $Co(OH)_2$, was observed on the electrodeposited samples after drying at 40 °C (Inset of

Figure 1). In addition, it should be emphasized that the applied potential and synthesis time in this study were optimized on the basis of some of our previous works on the electrodeposition of hydrotalcite-like compounds and CeO_2 [8, 9, 27, 34]. Applied potential at -1.2 V vs SCE could reduce the contribution of hydrogen evolution reaction, which decreased the stability of the coating. While the synthesis duration was adjusted to avoid excessive precipitation of the coating materials causing pore blockage in the foam., iIt was observed that, as the concentration of the electrolyte increased, the precipitation was promoted. Therefore, the time of precipitation was reduced to 500, 1000, and 1500 s for 0.15, 0.10, and 0.06 M electrolytes, respectively. Hence the most challenging issue of conventional dip-coating (removal of excess liquid-like by withdrawal) on small pore foams could be overcome by adjusting the synthesis time during the electrosynthesis even when thick coatings are prepared (vide infra).

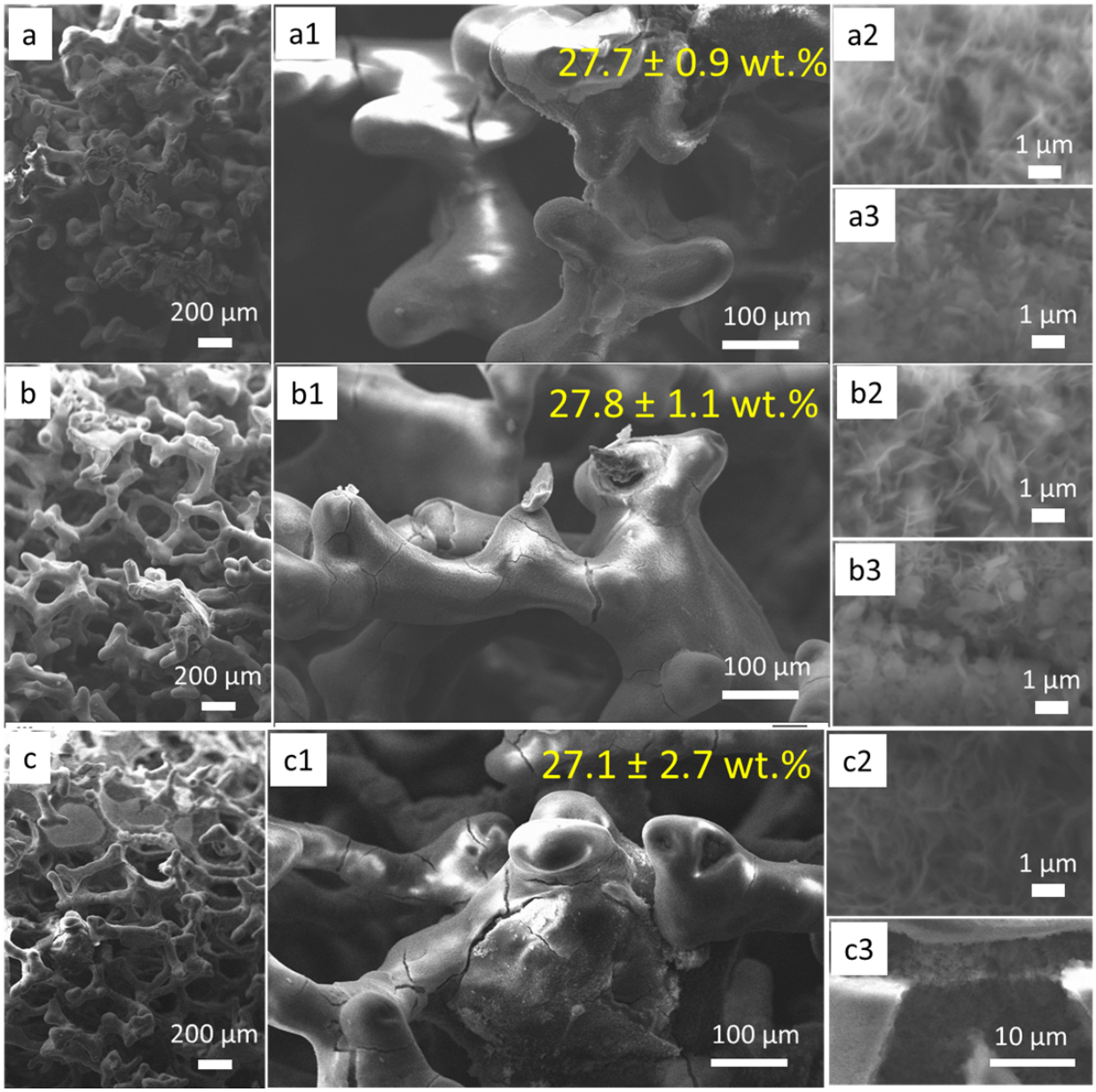

Figure 2. SEM images of electrodeposited samples (foam type I) prepared at -1.2 *V vs SCE* in different concentration of $Co(NO_3)_2$ electrolytes and synthesis duration: 0.06 M, 1500 s (a, a1, a2, a3); 0.10 M, 1000 s (b, b1, b2, b3); and 0.15 M, 500 s (c, c1, c2, c3). Figures a2, b2, and c2 showed the morphology of the second layer (top layer) while Figures a3 and b3 showed that of the first layer (bottom layer near foam surface). Figure c3 showed a crack with two different morphologies. Values of loadings were taken on an average of four replicated experiments.

To investigate the morphology of the coating, SEM analyses were carried out and the images at different magnifications of the foams electrodeposited in the three electrolytes were displayed in Figure 2. The concentration of electrolyte can influence the morphology of the hydroxide particles and thus of the coating [28]. The foam surfaces were fully covered by compact and almost crack-free blue layers with solid loadings, regardless of the synthesis conditions studied, of approximately 27 – 28 wt.% (Figure 2a1, b1, and c1). In some locations, cracks allowed to estimate the layer thickness to be about 15-18 μm, which was much thicker than those around 4-5 μm previously reported for electrodeposited $Co(OH)_2$ [12, 13]. These coatings were composed of 100 to 300 nm nanoparticles with a needle-like morphology (Fig. 2A2, b2, and c2) typical of α-$Co(OH)_2$ electrodeposited on Ni foam [13] or stainless steel plate [12]. Analyzing the zones where cracks developed, regardless of the electrodeposition conditions, it was observed that a layer near the foam surface showed larger particle size (Fig. 2A3, 2b3, and 2c3) than that of the top layer (Fig. 2A2, 2b2, and 2c2). This behavior suggests that the synthesis conditions used in this work did result in similar values of loading and morphology of the coating.

After calcination at 600 ^{o}C for 6 h, the loading decreased to 15 – 18 wt.% due to water and NO_x removal. During thermal treatment, some narrow cracks developed, though the coating was still stable, Figure 3a-c. The needle-like morphology was maintained, but larger particle sizes (about 200 – 400 nm) were observed in the layers (Figure 3a1-c1) in comparison to the as-synthesized sample (Figure 2). This is the normal sintering of particles under thermal treatment conditions [35].

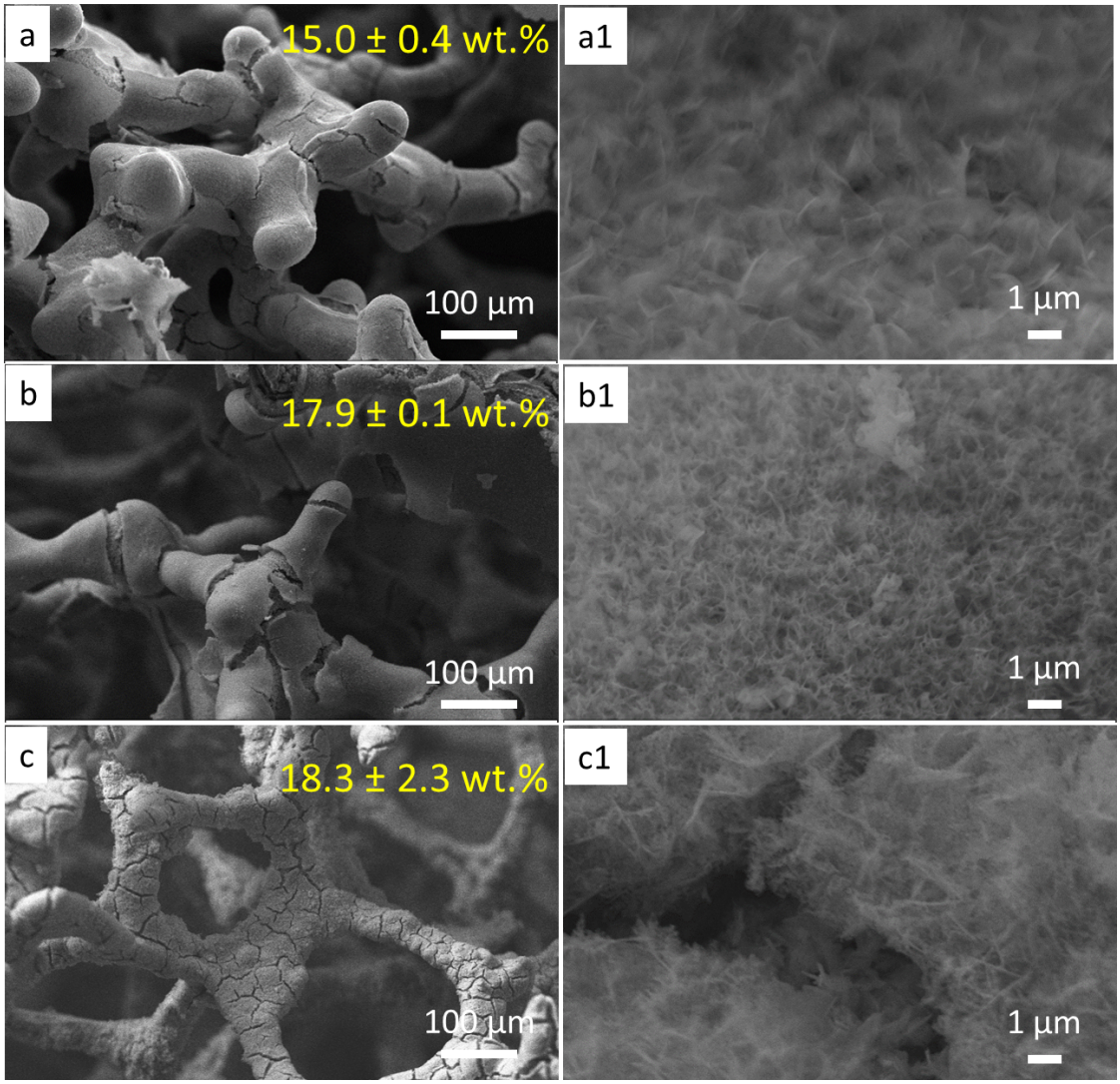

Figure 3. SEM images of Co_3O_4 structured catalysts (foam type I) prepared at -1.2 *V vs SCE* in different concentration of $Co(NO_3)_2$ electrolytes: 0.06 M-1500 s (a, a1); 0.10 M-1000 s (b, b1); and 0.15 M-500 s (c, c1). Calcination at 600 ^oC for 6 h, temperature ramp 10 $^oC\ min^{-1}$. Values of loadings were taken on an average of four replicated experiments.

The electrosynthesis is also applied to coat Co_3O_4 on another type of FeCrAlloy foam (type II) with different dimensions (1.6 mm thickness x 9 mm diameter) and pore sizes (nominal cell size 450 µm), and the SEM images of the samples after electrosynthesis and after calcination are shown in Figure 4. It should be noted that the difference in dimension of the foam substrate requires an adjustment in the synthesis parameters to avoid the deposition of excess materials causing the blockage of the foam substrate. For example, the synthesis time was 250 s for this small foam type II. This was only half compared to that for foam type I while keeping the same concentration of the electrolyte (0.15 M) and applied potential (-1.2 V vs SCE). Both as-synthesized samples and calcined samples showed very similar morphology to those prepared on foam type I. The loading of the washcoat layer on the foam type II was approximately 10.6 and

7.3 wt.% for the as-synthesized and calcined samples, respectively. A lower loading on foam type II than foam type I was due to a shorter synthesis time.

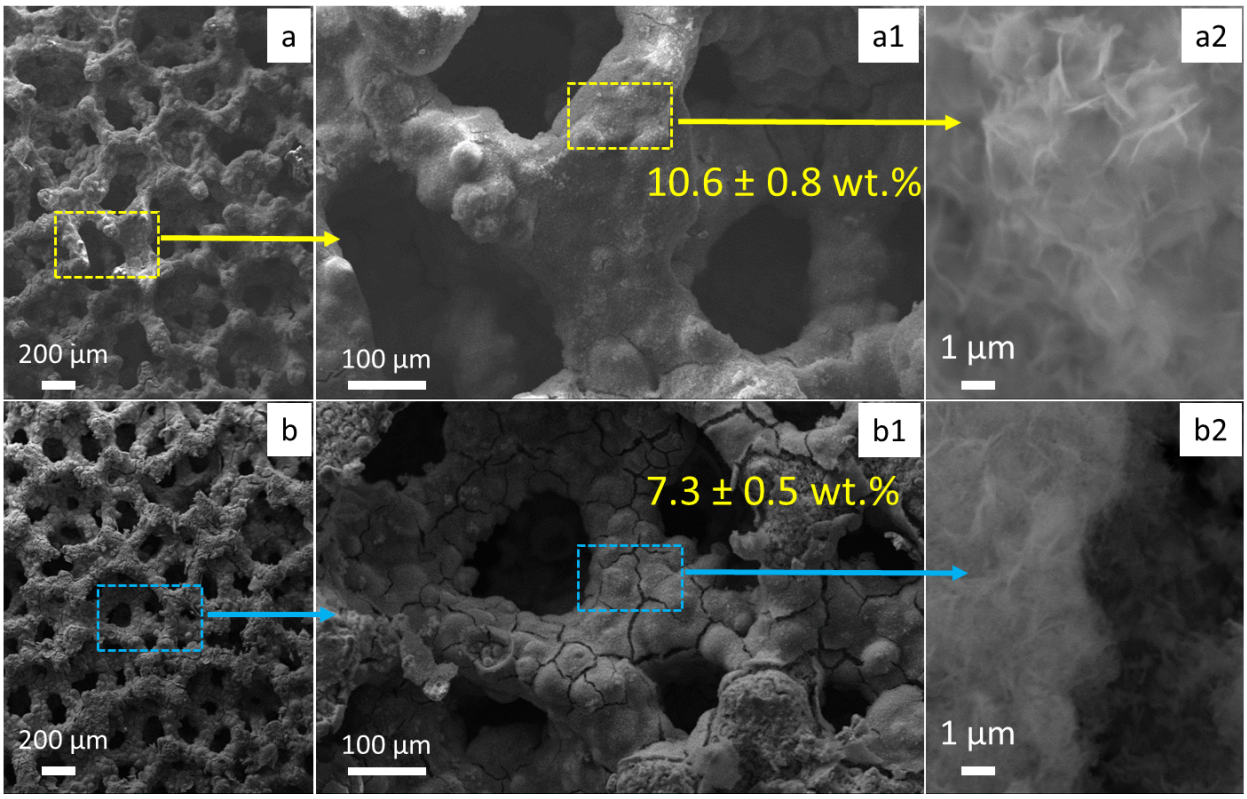

Figure 4. SEM images of Co_3O_4 coated on foam type II by the electrodeposition at -1.2 *V vs SCE* for 250 s in 0.15 M of $Co(NO_3)_2$ electrolyte: after electrodeposition (a, a1, a2) and after calcination at 600 °C for 6 h (b, b1, b2). Values of loadings were taken on an average of 12 replicated experiments.

The formation of a single cobalt hydroxide phase was expected [12], but despite several attempts, we were unable to record diffraction patterns in which the coating reflections were observed. This may be due to the poor crystallinity of the deposited phase rather than to a low amount of material, as we were able to record patterns for other coated foams (CeO_2, MgAl hydrotalcite-like compounds?) containing lower solid loadings [27, 34]. To obtain information about the crystalline nature of the solid deposited, the sample Co-0.15 was analyzed by micro-Raman, Figure 5. The two representative peaks of $Co(OH)_2$ were recorded at 518 and 451 cm^{-1}, which were associated with CoO (A_g) symmetric stretching and O-Co-O bending modes, respectively [36]. It was noted that from Raman spectra, two types of structures, namely, α-$Co(OH)_2$ and β-$Co(OH)_2$ could be identified by an intense band at 518 and 502 cm^{-1} Raman shift,

respectively. Therefore, the only presence of an intense band at 518 cm^{-1} without a band at 502 cm^{-1} in the Raman spectrum confirmed the α-$Co(OH)_2$ but not β-$Co(OH)_2$ structure in the as-electrodeposited sample [37]. In addition, the broad band centered at around 3600 cm^{-1} was attributed to the ν_{OH} of water and hydroxyl in the layer of $Co(OH)_2$ [38]. The sharp peak at 1051 cm^{-1} was assigned to the ν_1 symmetric stretching mode of NO_3^- species which could be both adsorbed or intercalated in $Co(OH)_2$ [39].

Raman spectra of the calcined catalyst showed five peaks assigned to the Co_3O_4 spinel structure. The most intense band at 679 cm^{-1} was related to the A_{1g} mode. The three peaks at 189, 514, and 609 cm^{-1} were associated with the F_{2g} mode, while the last one at 472 cm^{-1} was related to the E_g mode [40]. The absence of bands at 3600 and 1051 cm^{-1} confirmed that all hydroxides and nitrate were decomposed. The catalyst synthesized by precipitation also presented five peaks in the Raman spectrum, but only one peak at 188 cm^{-1} had the same Raman shift of Co structured catalyst, the other four peaks were shifted to lower values (Figure S2a). This indicated that there may be differences in the structure of Co spinel obtained from the two methods.

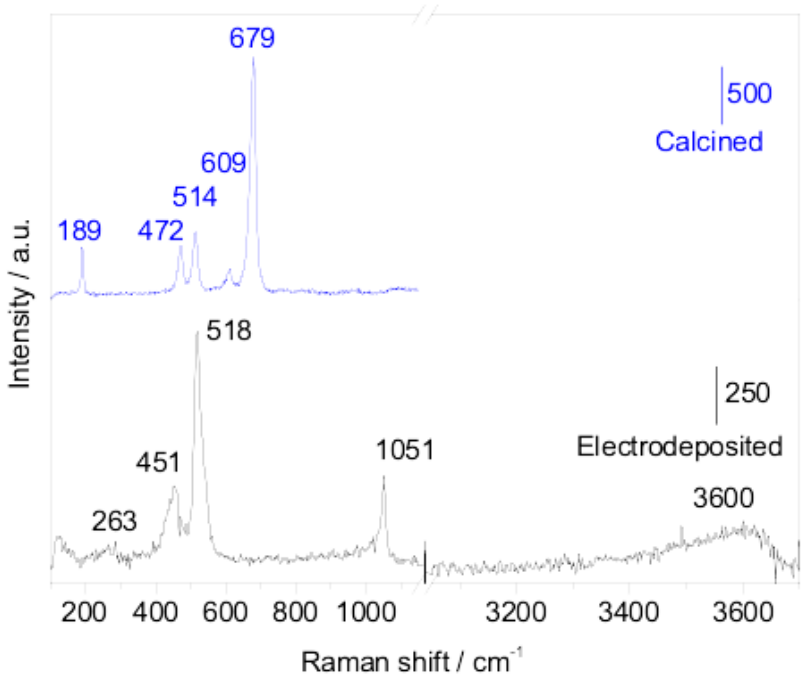

Figure 5. Raman spectra of Co-based structured catalysts (foam type I) prepared at -1.2 *V vs SCE* in 0.15 M $Co(NO_3)_2$ electrolytes for 500 s.

XRD patterns of the coated foams after calcination instead showed the reflections of the Co_3O_4 structure and the Fe of the foam (Figure 6). The crystallite size of Co_3O_4 calculated for the main reflection (plane (311) at 2θ of approximately 36.8º) using Scherrer's equation was about 35 nm.

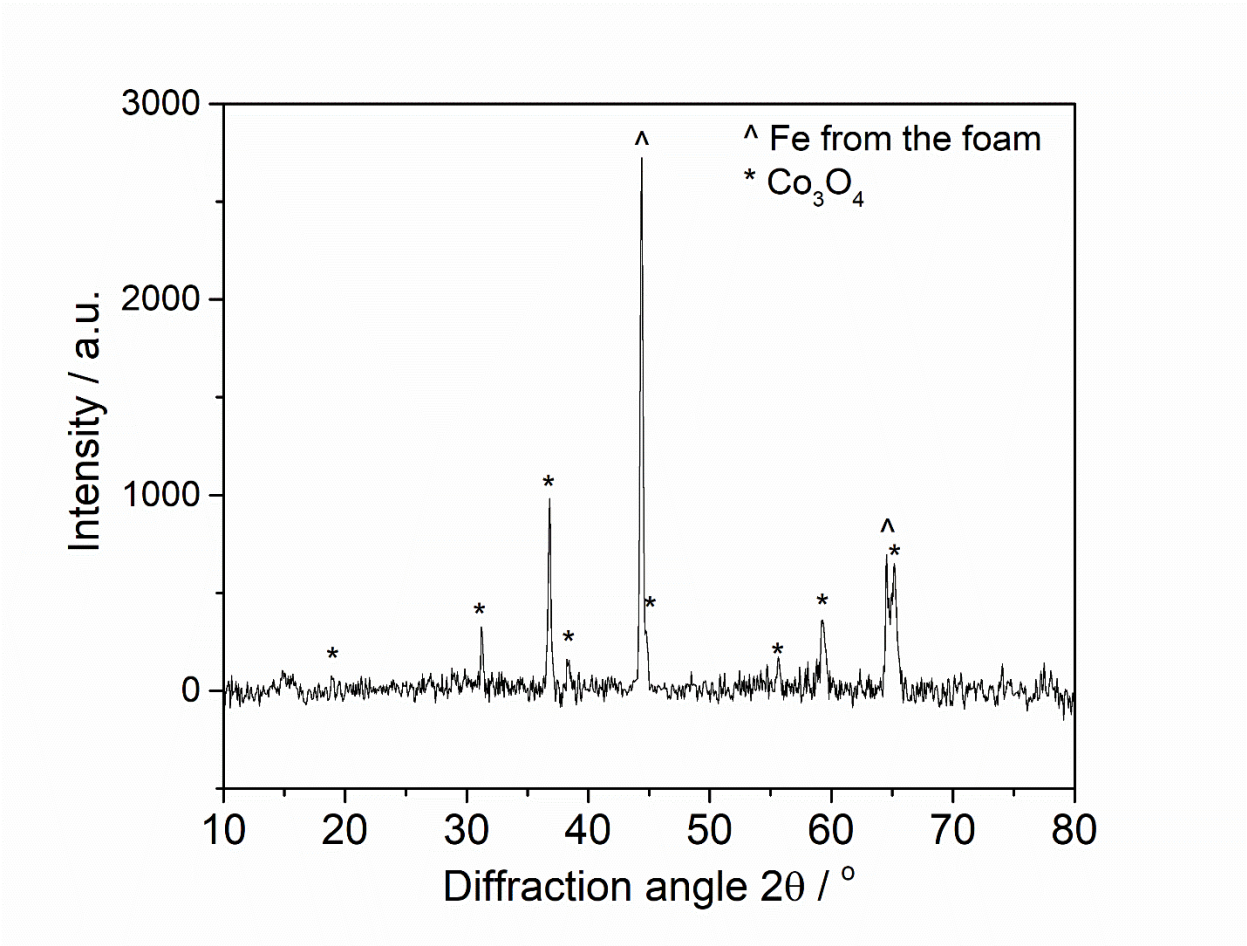

Figure 6. XRD pattern of Co_3O_4 coated on foam (type II) after calcination at 600 °C.

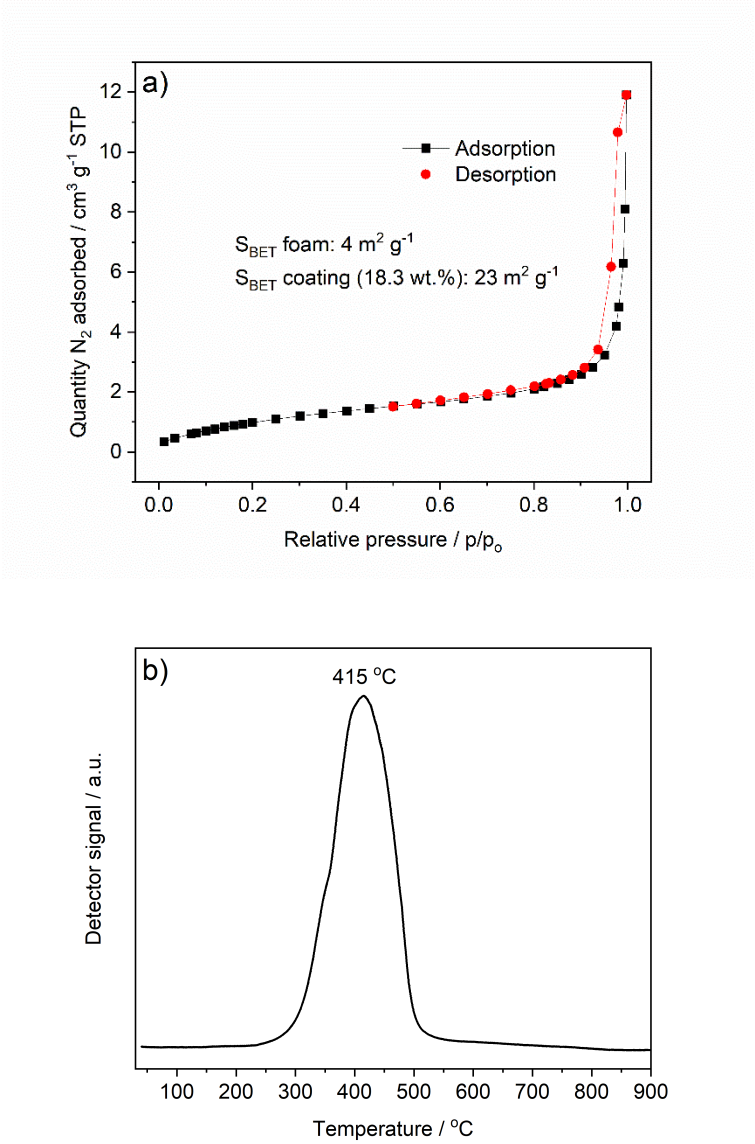

Figure 7. Characterization of Co-based structured catalysts (foam type I) prepared at -1.2 *V vs SCE* in 0.15 M $Co(NO_3)_2$ electrolytes for 500 s, and calcined at 600 °C for 6 h: a) isotherm nitrogen adsorption-desorption and b) H_2-TPR.

Figure 7a showed typical type IIb of N_2 adsorption-desorption isotherm on sample Co-0.15. This is characteristic of non-microporous materials with interparticle pores. The specific surface area determined by the BET method was about 4 m^2 g^{-1}, corresponding to 23 m^2 $g^{-1}_{coating}$. It is noted that the bare foam showed a negligible specific surface area. A similar specific surface area, 22 m^2 $g^{-1}_{coating}$ was measured for the Co-0.06 catalyst, suggesting that the synthesis conditions did not largely modify the textural properties of the resulting Co_3O_4 catalysts, in agreement with SEM images. It should be noted that these specific surface area values were significantly higher than for the Co_3O_4 powder catalyst prepared by thermal decomposition (4 m^2 g^{-1}) [41] or precipitation (10 m^2 g^{-1}, using $(NH_4)_2CO_3$ as precipitation agent and calcined at 700 °C for 3h) [42], as well as

than a commercial catalyst (Fluka 16 m^2 g^{-1}) [43]. Otherwise it was but lower than a precipitated sample calcined at 600 °C prepared by us in this work (25 m^2 g^{-1}, using NaOH) or from literature (30 m^2 g^{-1}, using $(NH_4)_2CO_3$) [44].

The reducibility of Co_3O_4 in Co-0.15 was analyzed by H_2-TPR and presented in Figure 7b. H_2 was consumed mainly in the range from 300 to 500 °C. The low-intensity shoulder at 350 °C could be associated with the reduction of Co_3O_4 to CoO, while the major peak at ca. 415 °C may be attributed to the reduction of bulk CoO to Co. The shape of the curves was similar to H_2-TPR profiles of Co_3O_4 prepared by combustion method [41] or of a commercial product [43] although the maximum temperature (T_{max}) again depended on the preparation method. Indeed, the T_{max} of the electrodeposited Co catalyst was lower (around 60 °C) than that of the combustion catalyst but higher than that of the commercial one. Compared to the precipitated catalyst, the electrosynthesis structured catalyst was easier to be reduced since the peaks were shifted to lower temperatures. The H_2-TPR profile of precipitated catalyst showed two distinct peaks around 406 and 520 which520, which were significantly higher than those of electrosynthesis catalyst (Figure S2b). This may be probably related to particle size because the small crystallite sizes are easier to be reduced than the big ones [45]. It was noted that the reducibility of the catalyst may influence its activity because the reduction of Co^{3+} to Co^{2+} by the desorption of oxygen is the determining step of the overall reaction rate [45]. The order of T_{max} was the same as the activity order during deN_2O.

3.2 N_2O catalytic decomposition

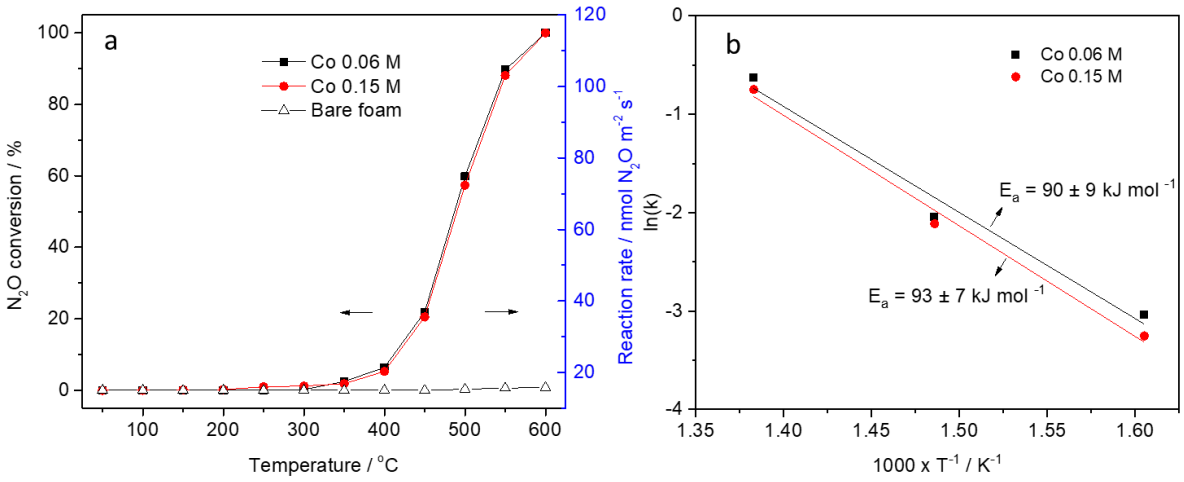

Figure 8. N_2O catalytic decomposition on Co structured catalysts (foam type I): a) N_2O conversion (left Y-axis) and reaction rate (right Y-axis); and b) Arrhenius plots for apparent activation energy calculation. Reaction conditions: two coated foams, GHSV = 6,800 h^{-1}, under 80 mL min^{-1} of 1000 ppm N_2O/N_2. Arrhenius plots used data points with conversion lower than 25% N_2O conversion. The error of the activation energy was calculated from the standard deviation value of the slope of the fitting curve.

For the N_2O decomposition, a pair of coated foams (type I, diameter 8 mm and height 7 mm) was loaded inside the quartz reactor. N_2O conversion and reaction rate of 0.1 vol.% N_2O/N_2 over Co-0.06 and Co-0.15 catalysts at temperatures 50 – 600 °C were presented in Figure 8a. A pair of bare foams calcined at 600 °C was also tested under the same reaction conditions for comparison purposes. The bare foam was inactive for N_2O decomposition up to 600 °C (conversion < 1%) as reported in our previous work [25]. Both Co-0.06 and Co-0.15 catalysts were active for deN_2O and their performance activity was almost identical. In both cases, N_2O started to be decomposed at 350 °C and converted completely at 600 °C. Klegova and co-workers reported the N_2O decomposition over Co_3O_4/open-cell SiC foam at the same N_2O concentration (1000 ppm) but lower GHSV (3000 h^{-1} *vs* 6800 h^{-1} in this work) [18]. Interestingly, comparable catalytic performances activity were obtained with their optimized sample, prepared by a suspension coating method, and our sample prepared by electrosynthesis: for example, at 450 ^oC almost the same 20% conversion of N_2O was measured, although a double GHSV was used in our study. However, it should be noted that both foam size (14 cm^3, diameter x length = 3 cm x 2 cm) and total flow rate (700 mL min^{-1}) were different from this study.

It is very challenging to compare N_2O decomposition performances activity of the structured and pelletized catalysts reported in the literature, due to dissimilarity in the reaction conditions. N_2O decomposition rate (r, also called turnover reaction rate TOR, nmol N_2O m^{-2} s^{-1}) may be an accurate assessment for such purpose [25]. The results of TOR for the structured catalysts used in this work are displayed in Figure 8a (right Y-axis). TOR of Co-based catalyst was 39 (nmol N_2O m^{-2} s^{-1}, at 490 °C), which was higher than the one of Co_3O_4 pelletized catalyst (less than 30 nmol N_2O m^{-2} s^{-1}, at 500 °C) reported by Kaczmarczyk et al. [42]. However, this value was lower than for a Co_3O_4 commercial powder catalyst (about 135 nmol N_2O m^{-2} s^{-1}, at 400 °C) reported by Maniak and coworkers [43]. It was worth noting that these results were performed underin different reaction conditions. In a work with more similar reaction conditions (0.3 g catalyst, 90 mL min^{-1} of 1000 ppm N_2O/N_2) performed on Co_3O_4 pelletized catalyst prepared by combustion method, Franken et al. [41] presented a TOR of 24.3 nmol N_2O m^{-2} s^{-1} (calculated at T_{50} around 550 ^oC).

To make a better comparison with pelletized catalysts, the Co_3O_4 catalyst prepared by precipitation was tested under the same concentration of N_2O (1000 ppm) and total flow rate (80 mL min^{-1}), but with 300 mg of catalyst. The N_2O conversion and reaction rate are shown in Figure S3. TOR at 490 ^oC was around 7.3 nmol N_2O m^{-2} s^{-1}. It can be therefore highlighted that a Co-based structured catalyst exhibited better TOR in comparison to Co_3O_4 pelletized catalyst prepared by combustion or precipitation method. This could be related to the high specific surface area, particle size, or reducibility, as reported for the effect of the preparation method of cobalt spinels on their N_2O decomposition activity [46, 47]. It should be noted that the internal diffusion limitation is also an important factor that needs to be considered for the comparison between the pelletized and structured catalysts. The coating layer of the structured catalyst (15-18 μm) is significantly thinner than the grain size of the pelletized catalyst (0.25-0.50 mm) and therefore it is expected the mass transfer limitation is lesser for the former than the latter. The

comparison of TOR of Co-based structured catalysts and other Co-containing catalysts in literature was summarized in Table 1.

Table 1. Comparison of turnover reaction rate between Co-based structured catalysts and Co-containing catalysts reported in literature.

Preparation method	S_{BET} ($m^2\ g^{-1}$)	T_{max} H_2-TPR (°C)	TOR (nmol $N_2O\ m^{-2}\ s^{-1}$)	Reference
Combustion	4	ca. 410, 480	24.3 (550 °C)	[41]
Commercial product	16*	ca. 415	135.0 (400 °C)	[43]
Precipitation	10	-	ca. 30.0 (500 °C)	[42]
Electrodeposition	23	ca. 350, 415	16.0 (450 °C) 39.0 (490 °C)	This work
Wet impregnation coating SiC foam	18	388, 436	11.8 (450 °C)	[18]
Suspension coating SiC foam	18	341, 448	18.3 (450 °C)	[18]

- from supplier

Apparent activation energies of Co-0.06 and Co-0.15 catalysts determined from the slope of linear regression fit of Arrhenius plots were displayed in Figure 8b. Both catalysts showed similar apparent activation energy of 90-93 kJ mol^{-1}. Interestingly, this value is almost the same as the raw value for Co_3O_4 precipitated catalysts calculated by Yu and co-workers. However, the authors corrected this value to a lower one, taking into account the change of active phase with increasing temperature [48]. In addition, this apparent activation energy value was also similar to the one reported for Co_3O_4 coated on α-Al_2O_3-cordierite honeycomb monolith by combustion or impregnation method (~83 – 88 kJ mol^{-1}) [14]. Moreover, Stelmachowski and co-workers have reported that octahedral Co^{3+} ions are more active than tetrahedral Co^{2+} ions, since the former showed apparent activation energy around 15-17 kcal mol^{-1} (63 – 71 kJ mol^{-1}) while for the latter it was 27 – 28 kcal mol^{-1} (113 – 117 kJ mol^{-1}) [24]. The apparent activation energy of the electrosynthesis catalysts was between these values, which suggests that they may contain both types of active sites.

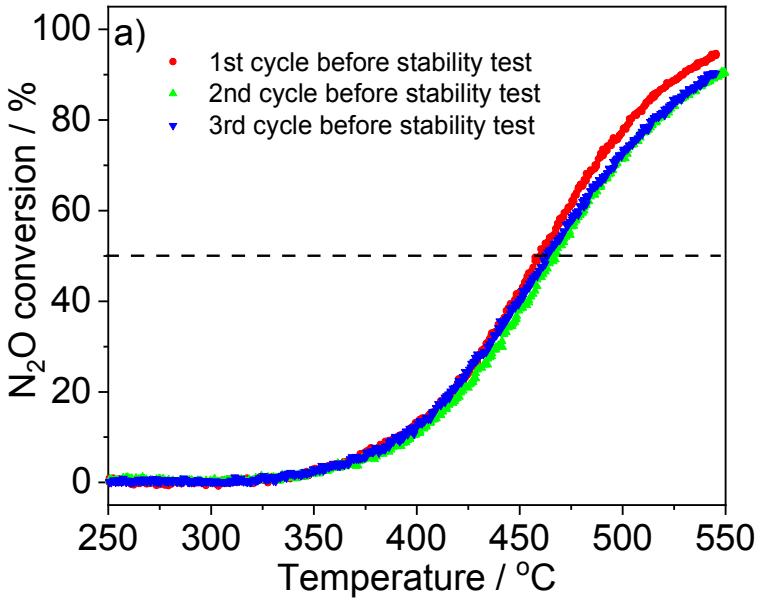
a)
1st cycle before stability test
2nd cycle before stability test
3rd cycle before stability test
N2O conversion / %
Temperature / °C
100
80
60
40
20
0
250
300
350
400
450
500
550

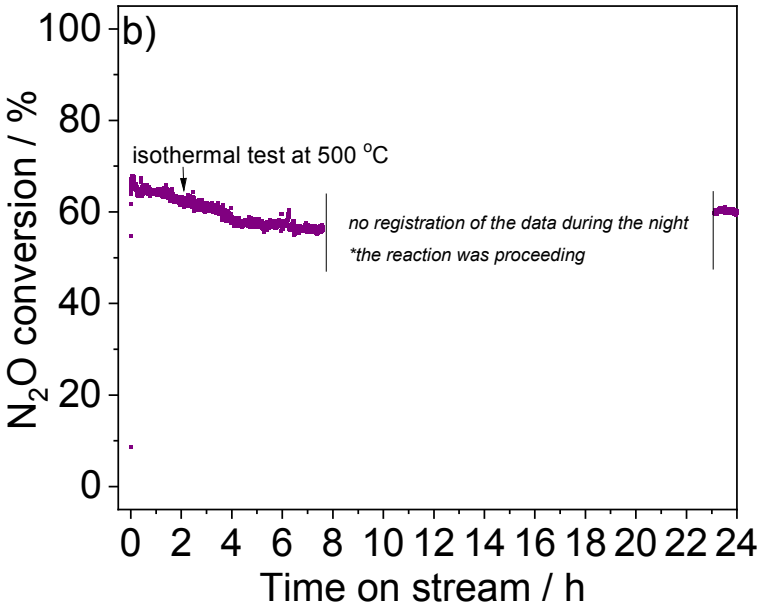
b)
isothermal test at 500 °C
no registration of the data during the night
*the reaction was proceeding
N2O conversion / %
Time on stream / h
100
80
60
40
20
0
0
2
4
6
8
10
12
14
16
18
20
22
24

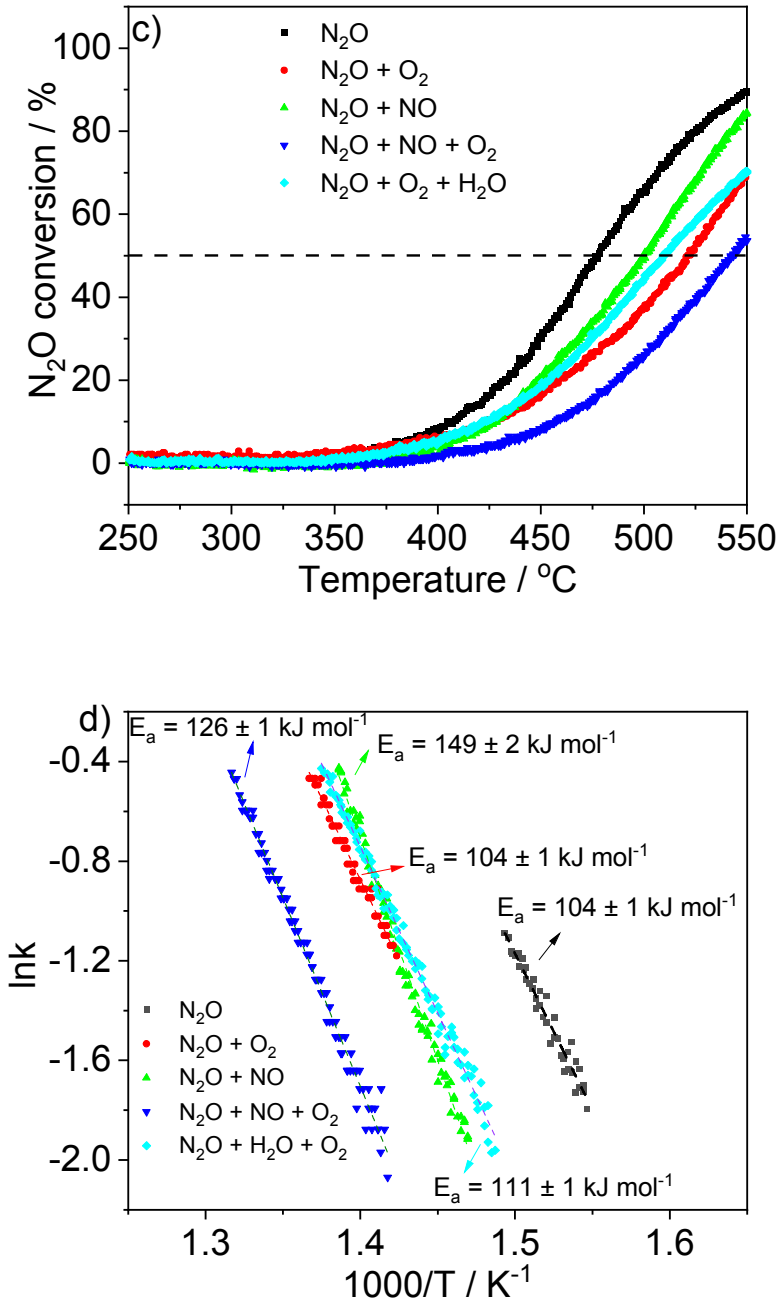

Figure 9. N_2O catalytic decomposition on Co-based structured catalysts (foam type II): a) cycle tests with TRSR; and b) stability test; c) effect of inhibitors; and d) Arrhenius plots for apparent activation energy calculation. Reaction conditions: five coated foams (total mass of coating 24 mg), GHSV = 3500 h^{-1} and WHSV = 75,000 mL $h^{-1}g^{-1}$ under 30 mL min^{-1} of 2500 ppm N_2O/N_2. The inhibitors were used with different concentrations including 500 ppm NO, 2% O_2, and 3.6

vol% H_2O. Arrhenius plots used data points with conversion lower than 20% N_2O conversion. The error of the activation energy was calculated from the standard deviation value of the slope of the fitting curve.

The structured catalyst using type II of FeCrAlloy foam was tested for N_2O decomposition with sequential experiments listed in Figure S1. Fig. 9A shows the conversion profiles of N_2O during three cycles of heating/cooling at a temperature range of 250 – 550 °C. The profiles of the second and the third cycle were almost identical and slightly lower than the profile of the first cycle in the temperature range from 450 to 550 °C. The T_{50} values of three cycles were in the range of 460 – 465 °C. Such a small difference in T_{50} values suggested that the activity of the catalyst was stable during the cycle tests. After the third cycle, the catalyst was tested at 500 °C for 24 h and the result is presented in Fig. 9b. The N_2O conversion decreased from 65% to 58% in the first five hours and was then almost stable at the plateau of 58% till the end of the test. The activity tests were subsequently performed in the presence of NO, O_2, and H_2O to investigate the effect of inhibitors. As shown in Figure 9c, the T_{50} values were ranked in an increasing order of N_2O (477 °C) < N_2O + NO (500 °C) < N_2O + O_2 + H_2O (509 °C) < N_2O + O_2 (521 °C) < N_2O + NO + O_2 (543 °C). The inhibitors such as NO, O_2, and H_2O have competitive adsorption on the active sites with N_2O and consequently inhibit the activity of the deN_2O catalysts [49, 50]. To gain more information on the impact of the inhibitors, the apparent activation energy was calculated (Figure 9d). The presence of O_2 exhibited a similar E_a value to N_2O alone, suggesting that O_2 may not alter the reaction pathway. In contrast, the presence of NO resulted in the activation energy of 149 kJ mol^{-1} which[1], which is approximately 1.4 times higher than that of N_2O alone. Such a significant increase in the value of apparent activation energy indicated that NO strongly inhibited the studied reaction due to its substantially competitive adsorption with N_2O. The mixture of NO+O_2+N_2O and H_2O+O_2+N_2O resulted in the E_a of 126 and 111 kJ mol^{-1}, respectively. A higher Ea of the former than the latter suggests that NO inhibited the N_2O decomposition stronger than H_2O in the window temperature of around 500 °C in this study.

3.3 Characterizations of the spent catalysts

After catalytic tests, SEM images revealed that both the adherence and morphology of the layers on two types of foams were almost the same as in the calcined catalyst, without any expansion of the cracks (Figure 10a, a1, b, and b1). To verify whether there was a phase change after the reaction, the catalyst was additionally examined by the micro-Raman. Only the five peaks at 188 (F_{2g}), 468 (F_g), 510 (F_{2g}), 604 (F_{2g}), and 670 (A_{1g}) cm^{-1} associated with cubic Co_3O_4 structure were observed in the Raman spectrum of the calcined samples (Figure 10c).

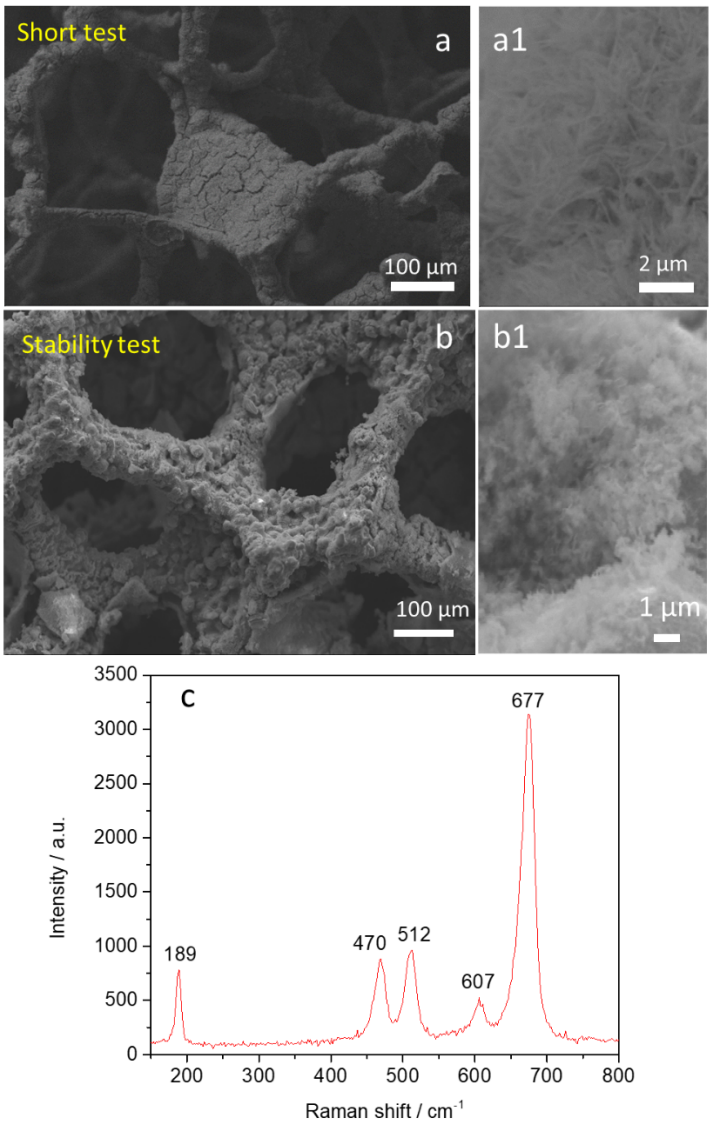

Figure 10. Characterization of the used Co-0.15M structured catalysts after the catalytic test: a and a1) SEM images of foam type I; b and b1) SEM images of foam type II, and c) Raman spectrum of foam type I.

4. Conclusions

Co_3O_4 structured catalysts based on FeCrAlloy open-cell foams were prepared by the facile electrodeposition method, followed by calcination at 600 ºC. The loading of coating can be adjusted by tailoring the synthesis parameters such as time and concentration. Stable Co_3O_4 layers were obtained on small pore foams without any pore blockage on different types of FeCrAlloy foams (7 mm x 8mm cylinder of 80 PPI and 1.6 mm x 9 mm of 450 µm cell size). The catalysts showed satisfactory performance for catalytic decomposition of N_2O with T_{50} around 490 ºC and a reaction rate of 39 nmol N_2O m^{-2} s^{-1} at 450 ºC. The structured catalyst showed a higher reaction rate than Co_3O_4 powder prepared by precipitation or combustion

method. The catalyst also performed a stable conversion of N_2O during a stability test of 24 h. The presence of inhibitors such as O_2, NO, and H_2O hindered partially the conversion of N_2O, causing a shift of T_{50} toward higher temperatures. The wide range of applications of Co_3O_4 catalysts as well as the possibility of improving the activity by further doping the Co_3O_4 structure, also during the electrodeposition method, may increase the applicability of the structured catalysts developed here.

Acknowledgments

P.H. Ho acknowledged the SINCHEM Grant for financial support of the Ph.D. research fellowship. SINCHEM is a Joint Doctorate programme selected under the Erasmus Mundus Action 1 Programme (FPA 2013–0037). We would like to thank Poivair and Alantum for supplying the open-cell foams. M.J. acknowledges a DFG Research Grant JA 2998/2-1.

CRediT authorship contribution statement

Phuoc Hoang Ho: Methodology, Investigation, Writing – original draft, Visualization. **Katarzyna Świrk**: Investigation, Writing – review & editing. **Magdalena Jabłońska**: Writing – review & editing, Supervision. **Giancosimo Sanghez de Luna**: Investigation, Writing – review & editing. **Francesca Ospitali**: Resources. **Francesco Di Renzo**: Writing – review, Supervision. **Gérard Delahay**: Conceptualization, Writing – review, Supervision. **Giuseppe Fornasari**: Writing – review & editing. **Angelo Vaccari**: Writing – review & editing. **Regina Palkovits**: Writing – review, Supervision. **Patricia Benito**: Conceptualization, Writing – review, Supervision.

References

[1] P.H. Ho, M. Ambrosetti, G. Groppi, E. Tronconi, R. Palkovits, G. Fornasari, A. Vaccari, P. Benito, Chapter 15 – Structured Catalysts-Based on Open-Cell Metallic Foams for Energy and Environmental Applications, in: S. Albonetti, S. Perathoner, E.A. Quadrelli (Eds.) Studies in Surface Science and Catalysis, Elsevier2019, pp. 303-327.

[2] A. Montebelli, C.G. Visconti, G. Groppi, E. Tronconi, C. Cristiani, C. Ferreira, S. Kohler, Methods for the catalytic activation of metallic structured substrates, Catalysis Science & Technology, 4 (2014) 2846-2870.

[3] E. Tronconi, G. Groppi, C.G. Visconti, Structured catalysts for non-adiabatic applications, Current Opinion in Chemical Engineering, 5 (2014) 55-67.

[4] M. Ambrosetti, R. Balzarotti, C. Cristiani, G. Groppi, E. Tronconi, The Influence of the Washcoat Deposition Process on High Pore Density Open Cell Foams Activation for CO Catalytic Combustion, Catalysts, 8 (2018) 510.

[5] A. Montebelli, C.G. Visconti, G. Groppi, E. Tronconi, S. Kohler, H.J. Venvik, R. Myrstad, Washcoating and chemical testing of a commercial Cu/ZnO/Al2O3 catalyst for the methanol synthesis over copper open-cell foams, Applied Catalysis A: General, 481 (2014) 96-103.

[6] F.J. Echave, O. Sanz, M. Montes, Washcoating of microchannel reactors with PdZnO catalyst for methanol steam reforming, Applied Catalysis A: General, 474 (2014) 159-167.

[7] L.F. Bobadilla, A. Muñoz-Murillo, O.H. Laguna, M.A. Centeno, J.A. Odriozola, Does shaping catalysts modify active phase sites? A comprehensive in situ FTIR spectroscopic study on the performance of a model Ru/Al2O3 catalyst for the CO methanation, Chemical Engineering Journal, 357 (2019) 248-257.

[8] P. Benito, G. Nuyts, M. Monti, W. De Nolf, G. Fornasari, K. Janssens, E. Scavetta, A. Vaccari, Stable Rh particles in hydrotalcite-derived catalysts coated on FeCrAlloy foams by electrosynthesis, Applied Catalysis B: Environmental, 179 (2015) 321-332.

[9] P.H. Ho, M. Ambrosetti, G. Groppi, E. Tronconi, J. Jaroszewicz, F. Ospitali, E. Rodríguez-Castellón, G. Fornasari, A. Vaccari, P. Benito, One-step electrodeposition of Pd–CeO2 on high pore density foams for environmental catalytic processes, Catalysis Science & Technology, 8 (2018) 4678-4689.

[10] H.S. Jeon, M.S. Jee, H. Kim, S.J. Ahn, Y.J. Hwang, B.K. Min, Simple Chemical Solution Deposition of Co3O4 Thin Film Electrocatalyst for Oxygen Evolution Reaction, ACS Applied Materials & Interfaces, 7 (2015) 24550-24555.

[11] P.T. Babar, A.C. Lokhande, B.S. Pawar, M.G. Gang, E. Jo, C. Go, M.P. Suryawanshi, S.M. Pawar, J.H. Kim, Electrocatalytic performance evaluation of cobalt hydroxide and cobalt oxide thin films for oxygen evolution reaction, Applied Surface Science, 427 (2018) 253-259.

[12] V. Gupta, T. Kusahara, H. Toyama, S. Gupta, N. Miura, Potentiostatically deposited nanostructured α-Co(OH)2: A high performance electrode material for redox-capacitors, Electrochemistry Communications, 9 (2007) 2315-2319.

[13] W.-J. Zhou, M.-W. Xu, D.-D. Zhao, C.-L. Xu, H.-L. Li, Electrodeposition and characterization of ordered mesoporous cobalt hydroxide films on different substrates for supercapacitors, Microporous and Mesoporous Materials, 117 (2009) 55-60.

[14] S. Wójcik, G. Ercolino, M. Gajewska, C.W.M. Quintero, S. Specchia, A. Kotarba, Robust Co3O4|α-Al2O3|cordierite structured catalyst for N2O abatement – Validation of the SCS method for active phase synthesis and deposition, Chemical Engineering Journal, 377 (2019) 120088.

[15] C.P. Rodrigues, V.T. da Silva, M. Schmal, Partial oxidation of ethanol over cobalt oxide based cordierite monolith catalyst, Applied Catalysis B: Environmental, 96 (2010) 1-9.

[16] M. Assebban, Z.-Y. Tian, A. El Kasmi, N. Bahlawane, S. Harti, T. Chafik, Catalytic complete oxidation of acetylene and propene over clay versus cordierite honeycomb monoliths without and with chemical vapor deposited cobalt oxide, Chemical Engineering Journal, 262 (2015) 1252-1259.

[17] L. del Río, G. Marbán, Stainless steel wire mesh-supported potassium-doped cobalt oxide catalysts for the catalytic decomposition of nitrous oxide, Applied Catalysis B: Environmental, 126 (2012) 39-46.

[18] A. Klegova, A. Inayat, P. Indyka, J. Gryboś, Z. Sojka, K. Pacultová, W. Schwieger, A. Volodarskaja, P. Kuśtrowski, A. Rokicińska, D. Fridrichová, L. Obalová, Cobalt mixed oxides deposited on the SiC open-cell foams for nitrous oxide decomposition, Applied Catalysis B: Environmental, 255 (2019) 117745.

[19] K. Pacultová, A. Klegova, T. Kiška, D. Fridrichová, A. Martaus, A. Rokicińska, P. Kuśtrowski, L. Obalová, Effect of support on the catalytic activity of Co3O4-Cs deposited on open-cell ceramic foams for N2O decomposition, Materials Research Bulletin, 129 (2020) 110892.

[20] C.W. Moncada Quintero, G. Ercolino, A. Poozhikunnath, R. Maric, S. Specchia, Analysis of heat and mass transfer limitations for the combustion of methane emissions on PdO/Co3O4 coated on ceramic open cell foams, Chemical Engineering Journal, 405 (2021) 126970.

[21] J.-I. Yang, J.H. Yang, H.-J. Kim, H. Jung, D.H. Chun, H.-T. Lee, Highly effective cobalt catalyst for wax production in Fischer–Tropsch synthesis, Fuel, 89 (2010) 237-243.

[22] Y. Liu, D. Edouard, L.D. Nguyen, D. Begin, P. Nguyen, C. Pham, C. Pham-Huu, High performance structured platelet milli-reactor filled with supported cobalt open cell SiC foam catalyst for the Fischer–Tropsch synthesis, Chemical Engineering Journal, 222 (2013) 265-273.

[23] J.C. Park, N.S. Roh, D.H. Chun, H. Jung, J. Yang, II, Cobalt catalyst coated metallic foam and heat-exchanger type reactor for Fischer–Tropsch synthesis, Fuel Processing Technology, 119 (2014) 60-66.

[24] A. Egaña, O. Sanz, D. Merino, X. Moriones, M. Montes, Fischer–Tropsch Synthesis Intensification in Foam Structures, Industrial & Engineering Chemistry Research, 57 (2018) 10187-10197.

[25] P.H. Ho, M. Jabłońska, R. Palkovits, E. Rodríguez-Castellón, F. Ospitali, G. Fornasari, A. Vaccari, P. Benito, N2O catalytic decomposition on electrodeposited Rh-based open-cell metallic foams, Chemical Engineering Journal, 379 (2020) 122259.

[26] Climate Change 2022, Mitigation of Climate Change, Summary for policymakers, 2021.

[27] P.H. Ho, W. de Nolf, F. Ospitali, A. Gondolini, G. Fornasari, E. Scavetta, D. Tonelli, A. Vaccari, P. Benito, Coprecipitated-like hydrotalcite-derived coatings on open-cell metallic foams by electrodeposition: Rh nanoparticles on oxide layers stable under harsh reaction conditions, Applied Catalysis A: General, 560 (2018) 12-20.

[28] P.H. Ho, E. Scavetta, F. Ospitali, D. Tonelli, G. Fornasari, A. Vaccari, P. Benito, Effect of metal nitrate concentration on the electrodeposition of hydrotalcite-like compounds on open-cell foams, Applied Clay Science, 151 (2018) 109-117.

[29] M. Rutkowska, Z. Piwowarska, E. Micek, L. Chmielarz, Hierarchical Fe-, Cu- and Co-Beta zeolites obtained by mesotemplate-free method. Part I: Synthesis and catalytic activity in N2O decomposition, Microporous and Mesoporous Materials, 209 (2015) 54-65.

[30] P. Stelmachowski, G. Maniak, J. Kaczmarczyk, F. Zasada, W. Piskorz, A. Kotarba, Z. Sojka, Mg and Al substituted cobalt spinels as catalysts for low temperature deN2O—Evidence for octahedral cobalt active sites, Applied Catalysis B: Environmental, 146 (2014) 105-111.

[31] P.H. Ho, M. Monti, E. Scavetta, D. Tonelli, E. Bernardi, L. Nobili, G. Fornasari, A. Vaccari, P. Benito, Reactions involved in the electrodeposition of hydrotalcite-type compounds on FeCrAlloy foams and plates, Electrochimica Acta, 222 (2016) 1335-1344.

[32] D.R.L. (ed), CRC Handbook of Chemistry and Physics, 84 th ed., 2003. Section 12, Properties of Solids, Electrical Resistivity of Pure Metals CRC Press, Boca Raton, Florida, (2003).

[33] F. Basile, P. Benito, G. Fornasari, V. Rosetti, E. Scavetta, D. Tonelli, A. Vaccari, Electrochemical synthesis of novel structured catalysts for H2 production, Applied Catalysis B: Environmental, 91 (2009) 563-572.

[34] P.H. Ho, M. Ambrosetti, G. Groppi, E. Tronconi, G. Fornasari, A. Vaccari, P. Benito, Electrodeposition of CeO2 and Pd-CeO2 on small pore size metallic foams: Selection of deposition parameters, Catalysis Today, 334 (2019) 37-47.

[35] E. Valatka, I. KelpŠAitĖ, J. BaltruŠAitis, Electrochemical Deposition of Porous Cobalt Oxide Films on AISI 304 Type Steel, Materials Science, 17 (2011).

[36] J. Yang, H. Liu, W.N. Martens, R.L. Frost, Synthesis and Characterization of Cobalt Hydroxide, Cobalt Oxyhydroxide, and Cobalt Oxide Nanodiscs, The Journal of Physical Chemistry C, 114 (2010) 111-119.

[37] J. Rahbani, N.M. Khashab, D. Patra, M. Al-Ghoul, Kinetics and mechanism of ionic intercalation/de-intercalation during the formation of α-cobalt hydroxide and its polymorphic transition to β-cobalt hydroxide: reaction–diffusion framework, Journal of Materials Chemistry, 22 (2012) 16361-16369.

[38] J.D. Pasteris, O. Beyssac, Welcome to Raman Spectroscopy: Successes, Challenges, and Pitfalls, Elements, 16 (2020) 87-92.

[39] A. Ianoul, T. Coleman, S.A. Asher, UV Resonance Raman Spectroscopic Detection of Nitrate and Nitrite in Wastewater Treatment Processes, Analytical Chemistry, 74 (2002) 1458-1461.

[40] V.G. Hadjiev, M.N. Iliev, I.V. Vergilov, The Raman spectra of Co₃O₄, Journal of Physics C: Solid State Physics, 21 (1988) L199-L201.

[41] T. Franken, R. Palkovits, Investigation of potassium doped mixed spinels CuxCo3−xO4 as catalysts for an efficient N2O decomposition in real reaction conditions, Applied Catalysis B: Environmental, 176-177 (2015) 298-305.

[42] J. Kaczmarczyk, F. Zasada, J. Janas, P. Indyka, W. Piskorz, A. Kotarba, Z. Sojka, Thermodynamic Stability, Redox Properties, and Reactivity of Mn3O4, Fe3O4, and Co3O4 Model Catalysts for N2O Decomposition: Resolving the Origins of Steady Turnover, ACS Catalysis, 6 (2016) 1235-1246.

[43] G. Maniak, P. Stelmachowski, A. Kotarba, Z. Sojka, V. Rico-Pérez, A. Bueno-López, Rationales for the selection of the best precursor for potassium doping of cobalt spinel based deN2O catalyst, Applied Catalysis B: Environmental, 136-137 (2013) 302-307.

[44] G. Ercolino, A. Grodzka, G. Grzybek, P. Stelmachowski, S. Specchia, A. Kotarba, The Effect of the Preparation Method of Pd-Doped Cobalt Spinel on the Catalytic Activity in Methane Oxidation Under Lean Fuel Conditions, Topics in Catalysis, 60 (2017) 333-341.

[45] Ž. Chromčáková, L. Obalová, F. Kovanda, D. Legut, A. Titov, M. Ritz, D. Fridrichová, S. Michalik, P. Kuśtrowski, K. Jirátová, Effect of precursor synthesis on catalytic activity of Co3O4 in N2O decomposition, Catalysis Today, 257 (2015) 18-25.

[46] M.A. Zamudio, S. Bensaid, D. Fino, N. Russo, Influence of the MgCo2O4 Preparation Method on N2O Catalytic Decomposition, Industrial & Engineering Chemistry Research, 50 (2011) 2622-2627.

[47] G. Grzybek, S. Wójcik, K. Ciura, J. Gryboś, P. Indyka, M. Oszajca, P. Stelmachowski, S. Witkowski, M. Inger, M. Wilk, A. Kotarba, Z. Sojka, Influence of preparation method on dispersion of cobalt spinel over alumina extrudates and the catalyst deN2O activity, Applied Catalysis B: Environmental, 210 (2017) 34-44.

[48] H. Yu, X. Wang, Apparent activation energies and reaction rates of N2O decomposition via different routes over Co3O4, Catalysis Communications, 106 (2018) 40-43.

[49] S.K. Mahammadunnisa, T. Akanksha, K. Krushnamurty, C.H. Subrahmanyam, Catalytic decomposition of N2O over CeO2 supported Co3O4 catalysts, Journal of Chemical Sciences, 128 (2016) 1795-1804.

[50] Y. Xiong, Y. Zhao, X. Qi, J. Qi, Y. Cui, H. Yu, Y. Cao, Strong Structural Modification of Gd to Co3O4 for Catalyzing N2O Decomposition under Simulated Real Tail Gases, Environmental Science & Technology, 55 (2021) 13335-13344.